



# Interhemispheric perspective on the most extreme surface winds in the storm tracks

Aleksa Stanković<sup>1,2</sup>, Rodrigo Caballero<sup>1,2</sup>, and Gabriele Messori<sup>1,3,4</sup>

<sup>1</sup>Department of Meteorology, Stockholm University, Stockholm, Sweden

<sup>2</sup>Bolin Centre for Climate Research, Stockholm University Stockholm, Sweden

<sup>3</sup>Department of Earth Sciences, Uppsala University, Uppsala, Sweden

<sup>4</sup>Swedish Centre for Impacts of Climate Extremes (climes), Uppsala University, Uppsala, Sweden

**Correspondence:** Aleksa Stanković (aleksa.stankovic@misu.su.se)

**Abstract.** Extratropical cyclones occur most frequently over the oceans, where they cause the strongest extreme surface winds. In this study, we investigate extreme surface winds during winter months in the northern and southern hemisphere, when the wind storms are the strongest. The analysis focuses on storm tracks over the North Atlantic, North Pacific and Southern Ocean.

5 We use ERA5 reanalysis data to make composites of extratropical cyclones that cause the top 100 most extreme surface wind events from 1979 until 2020 ("top 100 extremes"). We focus on large-scale atmospheric processes and find that the most prominent large-scale feature of the top 100 extremes in each basin is the presence of a pre-existing downstream cyclone a few days before the time of the maximum surface winds. Pre-existing cyclones are situated poleward and eastward of the top 100 extremes and their presence is consistent with strong upper-level winds and potential vorticity anomalies. Differences between  
10 the basins and hemispheres are quantitative. The top 100 extremes in the northern hemisphere develop in an environment with higher mid-tropospheric Eady growth rates, higher deepening rates and stronger surface wind speeds around the cyclones than in the southern hemisphere. Furthermore, we run the general circulation model ISCA with different boundary conditions to investigate their influence on the basin-wide extreme surface winds. We find a strong positive correlation between basin-wide extremes in mid-tropospheric Eady growth rates and surface winds. Zonalizing sea-surface temperatures across tropical and  
15 extratropical regions greatly reduces the differences in extreme surface winds between the North Atlantic and North Pacific; inter-hemispheric differences in extreme surface winds between the North Atlantic and Southern Ocean are greatly reduced when sea-surface temperatures are zonalized globally and made hemispherically symmetric, and orography is flat.

## 1 Introduction

20 Extratropical cyclones (hereafter, cyclones) are associated with a variety of extreme weather events, including extreme precipitation and windstorms (e.g., Catto et al., 2012; Pfahl and Wernli, 2012; Dowdy and Catto, 2017). Cyclones most frequently occur over the oceans, in regions known as storm tracks. Surface winds associated with oceanic cyclones are crucial for air-sea interactions, generating ocean waves which help determine surface roughness (Donelan et al., 1993), and controlling turbulent fluxes of energy (Hsiung, 1986) and CO<sub>2</sub> (Wanninkhof and McGillis, 1999) between the atmosphere and the ocean. Oceanic surface winds are also important to marine ecosystems (Lacour et al., 2017) and to economic activities such as wind power



25 generation (Liu et al., 2008) and shipping (Cardone et al., 2015). Moreover, cyclones that develop over the oceanic storm tracks and make landfall pose a major socioeconomic hazard (e.g., Ulbrich et al., 2013a; Shimkus et al., 2017).

Here, our focus is on understanding the large-scale dynamical processes leading to extreme surface winds in midlatitudes. This improved understanding may ultimately help alleviate the biases and uncertainty that affect projections of extreme surface wind changes in future climates (Catto et al., 2019; Seneviratne et al., 2021). We are particularly interested in the relationship  
30 between extreme winds and the cyclones that drive them. We focus on the main ocean basins, where cyclones are most plentiful and free from the complexities of interaction with continental topography and surface roughness, making results more statistically significant and simpler to interpret physically.

We take a comparative approach, aiming to gain new insight by investigating similarities and differences between the major storm track regions. While the American and Eurasian landmasses confine the northern hemisphere (NH) storm tracks to form  
35 distinct North Atlantic (NA) and the North Pacific (NP) storm tracks, the limited land area of the southern hemisphere (SH), on the other hand, yields a single Southern Ocean (SO) storm track with weak zonal structure. Cyclones in all these ocean basins arise due to the same basic baroclinic instability process, but differences in surface boundary and upstream conditions in the different storm tracks influence their local statistics.

In particular, bulk metrics such as zonally-averaged, vertically-integrated eddy kinetic energy or median annual surface winds  
40 are larger in the SO than in the NH basins, which is why the SO is often considered the stormier hemisphere (Shaw et al., 2022; Chemke et al., 2022). However, *extreme* surface winds are stronger over the NH storm tracks (Stanković and Caballero, 2025), particularly the NA. This is true across reanalysis and observational products, and mainly stems from stronger extreme winds in the vicinity of winter cyclones in the NH. Hence, at least when measured by their surface wind speeds, extreme cyclone intensities are greater in the NH than in the SH.

45 Our aim in this study is to better understand the reasons for these opposite inter-hemispheric asymmetries in mean and extreme oceanic winds. We address the following specific questions:

1. What are the large-scale processes leading to the generation of cyclones causing extreme surface winds in each storm track?
2. What differences in these large-scale processes can help explain the greater frequency of extreme surface winds in the  
50 northern than in the southern hemisphere?
3. How are these dynamical differences related to differences in surface boundary conditions across the storm track basins?

We address these questions focusing on winter seasons, when cyclones are the strongest in both hemispheres, and we select the 100 historical cyclones associated with the strongest extreme surface winds in each storm track region (hereafter top 100 extremes). We analyze large-scale fields through time-lagged composite analysis. We then use an intermediate-complexity  
55 climate model to test the importance of different boundary conditions for explaining the hemispheric asymmetry in extreme surface winds. The data and methods we use are described in Sect. 2, after which we present our main results in Sect. 3. We discuss the results and provide the future outlook in Sect. 4 and finally summarize our main findings in Sect. 5.



## 2 Data and Methods

### 2.1 ERA5

60 We employ the ERA5 global atmospheric reanalysis from the European Centre for Medium Range Weather Forecasts (Hersbach et al., 2020) spanning 1979-2020 to study the most extreme historical cyclones. Even though the ERA5 reanalysis covers the period from 1940 to present day, we focus on the period after 1979 because it assimilates satellite observations which are crucial for robustly representing sparsely observed regions in the SH. On the other hand, we focus our analysis to the period up until 2020 because the output provided by the cyclone-tracking algorithm (described below) ends with 2020. The reanalysis  
65 has hourly temporal and  $0.25^\circ$  ( $\sim 31$  km) spatial resolution. We focus on the analysis of winter seasons, defined as December-February in the NH and June-August in the SH. We use surface windspeed calculated as  $(u_{10}^2 + v_{10}^2)^{1/2}$ , where  $u_{10}$  and  $v_{10}$  are 10-m zonal and meridional wind components taken from ERA5. We additionally consider 250 hPa wind speed, potential vorticity (PV) from 300 hPa to 200 hPa (4 vertical levels) and mean sea level pressure (MSLP). We further calculate the instantaneous, dry Eady growth rate as:  $EGR = 0.31 \frac{f}{N} \frac{\partial |\mathbf{u}|}{\partial z}$  between 500–850 hPa, calculated as in (Besson et al., 2021; Stanković  
70 and Caballero, 2025). Here  $f$  denotes Coriolis parameter,  $|\mathbf{u}|$  the magnitude of horizontal wind speed,  $z$  is the vertical coordinate and  $N = \sqrt{\frac{g}{\theta} \frac{\partial \theta}{\partial z}}$  the Brunt-Väisälä frequency, commonly used as a measure of static stability, with  $g$  being gravitational acceleration and  $\theta$  potential temperature. We use the instantaneous EGR to avoid biases connected to nonlinearities and covariances observed with time-mean EGR (Simmonds and Lim, 2009). Finally, our analysis includes vertically integrated eddy kinetic energy,  $EKE = \int_{p_1}^{p_2} \frac{u'^2 + v'^2}{2g} dp$ , where  $u'$  and  $v'$  are zonal and meridional deviations from local monthly means for  
75 each given month at each grid cell,  $p_1 = 1000$  hPa and  $p_2 = 200$  hPa.

### 2.2 Selection and tracking of top 100 extremes in each basin in ERA5

We identify storm tracks as areas where the annual 98th percentile of daily maximum surface windspeed exceeds  $18 \text{ m s}^{-1}$  in ERA5. This is the same criterion used in Stanković and Caballero (2025) and it identifies three separate storm track regions with comparable statistics, one each in the North Atlantic, North Pacific and Southern Ocean (see Fig. 1a). We use this criterion  
80 based on surface winds because our main scientific question is the understanding of surface wind extremes, but the storm tracks we identify coincide with storm tracks identified by using other measures (Hoskins and Hodges, 2002, 2005; Shaw et al., 2016). As our focus is on the large-scale dynamics, we repeat the procedure of Stanković and Caballero (2025) and exclude regions that are within 300 km distance from the coasts of Greenland and Antarctica which feature very strong surface winds primarily caused by mesoscale processes.

85 We identify cyclones in ERA5 using cyclone tracks produced by Beran et al. (2024). This feature-tracking algorithm applies topological methods (Engelke et al., 2021; Nilsson et al., 2022) to track MSLP minima in ERA5 and provides hourly global output. It improves the method of Hanley and Caballero (2012a) and it is primarily developed to better represent multi-centre cyclones. The same algorithm was previously used in Stanković and Caballero (2025). The choice of the tracking algorithm could potentially have an influence on the results. However, tracking intercomparison studies consistently show a strong agree-  
90 ment between different tracking algorithms in representing deep, well developed cyclones (Neu et al., 2013; Ulbrich et al.,



2013b; Messmer and Simmonds, 2021). Therefore, as our focus lies on some of the most extreme cyclones in each basin, we argue that results should not be overly sensitive to the choice of tracking algorithm.

To find the cyclones associated with the top 100 most extreme wind events in each basin (i.e. *top 100 extremes*), we calculate a meteorological wind severity index (severity) as follows:

$$95 \quad S = \sum_{i \in \text{footprint}} \left( \frac{v_i}{v_{98_i}} - 1 \right)^3 I(v_i, v_{98_i}), \quad (1)$$

where  $i$  indexes all the grid cells within the connected wind footprint,  $v_i$  is daily maximum 10-m wind speed at grid point  $i$ ,  $v_{98_i}$  is the local 98th percentile with respect to the winter climatology from 1979 to 2020, and  $I(a, b) = 1$  if  $a > b$  and 0 otherwise. This index, or similar forms of it, have long been used to study windstorms associated with cyclones (e.g., Klawa and Ulbrich, 2003; Leckebusch et al., 2008; Hanley and Caballero, 2012b; Moemken et al., 2024). Although the wide-spread  
100 use of this index stems from its usefulness in modeling insurance-related windstorm losses, it also has physical grounding as the cube of the wind speed represents the flux of kinetic energy. Furthermore, it is reliant on an extreme percentile threshold which motivates its use for extreme weather analysis. Therefore, we use it to rank extreme wind events even though we are not directly interested in analyzing insurance losses. This same procedure was adopted in Stanković et al. (2024) to identify extreme windstorms over the central North Atlantic.

105 We calculate severity in each basin (defined by the masks described earlier) for each winter day and select daily maximum values. Values of severity are calculated over contiguous regions of wind exceedances over the local 98th percentiles. As two or more cyclones can be simultaneously present in the same basin, there can be more than one value of severity in a given day in a given basin caused by different cyclones; in this case, we only select the maximum value of severity for that day. We analyze contiguous regions in order to more robustly assign wind extremes to cyclones that caused them, as the largest part of severity  
110 caused by individual cyclones comes from contiguous regions in their vicinity (further explanation and a visual illustration of the method can be found in Fig. 2 of Stanković et al., 2024).

We select the 100 winter days with the highest severity in each basin. We examine the severity footprints during each of these days and find the highest daily surface windspeed within it. Then, based on the objectively identified cyclone tracks, we select the cyclone centre closest to the location of maximum windspeed and track the cyclone back in time.

### 115 2.3 Composite analysis

We compute cyclone-centered composites to identify the main large-scale flow features associated with the top 100 extremes in each basin. The convergence of latitude lines towards the poles necessitates regridding of meteorological fields to radial grids centered on the cyclone centers. To do this, we follow the grid transformation explained in detail in Appendix A of Bengtsson et al. (2007), often applied in studies like ours (e.g., Catto et al., 2010; Dacre et al., 2012; Laurila et al., 2021). Our composite  
120 analysis includes both the absolute values of the analyzed fields and their anomalies from the 1979-2020 climatology. We calculate climatologies by computing a 31-day running-mean of the daily means for calendar days of a given variable at every grid point and pressure level of interest. To test whether the anomalies from climatology are statistically significant, we construct for each basin and time step of interest, 30 randomly generated composites, each containing the same number of



125 fields as the original composite. These composites are made by retaining the original cyclone centers but assigning each to a randomly selected winter date. Thus, at  $t = 0$  d, the 30 composites collectively sample 3000 randomly selected dates. Anomalies are deemed statistically significant at the 1 % level after being corrected for false discovery (Wilks, 2016).

## 2.4 ISCA model and experiment setups

We perform sensitivity experiments using ISCA, an open-source modeling framework developed by Vallis et al. (2018). Our starting point is ISCA's default setup with realistic continents and prescribed sea-surface temperatures (SSTs) and ice fraction  
130 (Vallis et al., 2018). Prescribed SSTs and ice fraction used to force the model repeat annually, but vary monthly according to the monthly means of the years used in AMIP (Taylor, 2000). The model uses a spectral dynamical core to integrate the primitive equations. We run the model at T42 horizontal and hourly time resolution. The model parametrizes large-scale condensation and evaporation as in Frierson et al. (2006) and Vallis et al. (2018), radiation as in Clough et al. (2005) and also contains a simple representation of land and sea ice. It does not contain a representation of clouds, and instead assumes immediate  
135 precipitation with no explicit condensed water content in the atmosphere (Vallis et al., 2018). ISCA has been widely used to study different climates and is, in general, able to realistically represent Earth's climate (e.g., Vallis et al., 2018; Thomson and Vallis, 2018a, b; Patterson et al., 2020; White et al., 2024). More information about the model configuration is found in Vallis et al. (2018).

We first show that ISCA can be used to study wind extremes, as it represents well the annual and winter climatology of  
140 near-surface winds (see Fig. 1 and Sect. 3.2). We then vary boundary conditions to explore the effects they have on surface wind extremes over the storm track regions – a commonly used approach for studying storm track dynamics (e.g., Brayshaw et al., 2009, 2011; Shaw et al., 2016). We run 11 different experiments (the list of which can be found in the Supplementary Material), but focus our analysis on three experiments we find to be the most consequential. We also briefly discuss the most salient conclusions of the additional experiments in the Results section. The three experiments we focus on are:

- 145 – *Full*, which uses the realistic representation of orography and SSTs and is similar to the control set-up used by Patterson et al. (2020);
- *ZonalSST*, where SSTs are zonalized in both the tropics and extratropics by taking a longitudinal mean across all ocean grid cells over each latitude;
- *HemSymFlat*, where zonalized SSTs are also hemispherically symmetrized by prescribing SSTs of each latitude in the  
150 NH to a corresponding latitude in the SH while respecting seasonality (i.e., latitudes with the same absolute values have same SST values in the NH and in the SH during their respective winters) and orography is made flat.

All experiments are run for 15 years, with the first two years (four in cases where SSTs are hemispherically symmetrized) disregarded as a spin-up time. The prescribed SSTs are found and discussed later in the Results section. The boundary layer parametrization schemes in the ISCA model do not produce 10-m wind speed as the model output. We instead use the wind-  
155 speed at the level closest to the surface (973.1 hPa corresponds to the lowest full model level, diagnosed from ISCA's native



sigma-pressure vertical coordinate) and refer to winds at this level as surface winds when we discuss ISCA results. Storm track masks are constructed similar to ERA5. However, because surface winds in ISCA are at a higher level, where the effects of surface friction are smaller, we use a higher threshold of annual 98th percentile ( $21 \text{ m s}^{-1}$ ). Additionally, we do not exclude grid cells that are less than 300 km away from Greenland and Antarctica as in ERA5, since the much coarser resolution of the ISCA model does not resolve mesoscale features of these regions. We calculate a separate storm track mask for each ISCA experiment, in order to account for small changes in storm track areas due to the different boundary conditions.

### 3 Results

#### 3.1 Composite analysis of top 100 extremes in each basin in ERA5

Figure 2 shows the development of the top 100 extremes in each basin as lagged composites of MSLP anomalies from climatology. The figure shows that in each basin and across hemispheres, the development of top 100 extreme cyclones occurs in the presence of a pre-existing cyclone located downstream of the developing extreme cyclone. This result generalizes our previous finding on the presence of pre-existing cyclones around top extremes in the NA (Stanković et al., 2024) to all major storm track basins. Close to the time of cyclogenesis ( $t = -2 \text{ d}$ , Fig. 2a,d,g), these pre-existing downstream cyclones are poleward (note the reversal of the sign on y-axis on Fig. 2g-i for the SO's composites) and eastward of the extreme cyclone (located at the centre of each panel). The extreme cyclones display initially weak and spatially limited anomalies at  $t = -2 \text{ d}$ , which then grow in size and intensity as they approach the pre-existing downstream cyclone. At  $t = 0 \text{ d}$  (Fig. 2c,f,i), the two cyclones appear to merge and form a broad area of large negative MSLP anomalies. Thus, MSLP anomalies during the development of the top 100 extremes follow the same general pattern in all basins.

Composites of upper-level fields, like their surface counterparts, also show qualitative similarity across basins (Fig. 3). The pre-existing downstream cyclone advects high-PV air equatorward generating a region of high PV gradients, consistent with an intense jet streak and positive upper-level PV anomalies around the location of the developing extreme cyclone in the days leading to peak surface winds (Fig. 3). However, quantitative differences between the hemispheres are more prominent than for MSLP (cf. Figs. 2 and 3). Upper-level PV poleward of the top 100 extremes is greater in the NH than in the SH, making the PV gradient in the NH much larger than in the SH (which is also reflected in the stronger jet streaks). The strongest upper-level PV gradient and jet streak composites are found in the NP. Quantitative differences are also observed in the upper-level PV anomalies around cyclone centers of the top 100 extremes, which have larger values in the NH at  $t = 0 \text{ d}$  (Fig. 3c,f,i).

In summary, while the extreme cyclones in our sample follow a qualitatively similar large-scale development in all basins, those in the NH are accompanied by larger upper-level PV gradients and stronger jet streaks. Can these differences account for the climatological hemispheric asymmetry in extreme surface winds, characterized by stronger surface winds around NH cyclones (Stanković and Caballero, 2025)? We investigate this by exploring the time-evolution of medians of EGR, EKE and 10-m winds in the 1,000-km footprint around cyclone centers of the top 100 extremes.

As shown in Fig. 4, median values of these fields around the centers of top 100 extreme cyclones indicate that these are more intense in the NH than in the SH, whether measured by column-integrated EKE or 10-m winds. Furthermore, mid-tropospheric



EGR in the NH is consistently higher than in the SH in the days leading to peak severity (Fig. 4a). As the EGR is a proxy  
190 for the rate with which instabilities grow in a baroclinic atmosphere, higher EGR around a cyclone could, to first order, be  
understood as a greater potential for rapid intensification. This is supported by the time-evolution of cyclone intensity: the rate  
with which EKE rises between  $t = -2$  d and  $t = 0$  d is much greater in the NH (Fig. 4b). Consistently, there are almost twice as  
many explosively deepening cyclones among top 100 extremes in the NH than in the SO: 69% and 75% in the NA and the NP  
195 respectively compared to 38% in the SO, with explosively deepening cyclones defined as those experiencing a decrease of the  
normalized values of 24-hourly MSLP greater than 24 hPa (Sanders and Gyakum, 1980).

It appears therefore that the main difference between the top 100 extremes in different basins is a quantitative one, charac-  
terized primarily by the mid-tropospheric baroclinicity measured by EGR. The presence of a pre-existing downstream cyclone  
that acts as to intensify the upper-level PV gradient and the jet steak, as seen in the composite analysis, can consequently also  
intensify the EGR. Composites of EGR show that EGR has its highest values around the jet cores (Supplementary Material) and  
200 stronger jet cores observed in the NH are associated with stronger vertical wind shear. As the vertical wind shear is the main  
component driving the differences in EGR between the hemispheres (the stability term plays a smaller role, see Supplementary  
Material), the fact that the number of the top 100 extremes that deepen explosively is almost two times larger in the NH than  
in the SH can primarily be connected to the differences in the jet steak influenced by the presence of pre-existing downstream  
cyclones.

205 From a climatological perspective, winter basin-wide 98th percentiles of EGR correlate well with winter basin-wide 98th  
percentiles of 10-m winds, having the highest values in the NA, followed by the NP and then the SO (Supplementary Material).  
Furthermore, we note lower 10-m winds when we identify a new group of cyclones in each basin with lower median EGR in  
the 1,000-km footprint around the cyclone centers (so that the maximum during the cyclones' lifetimes is  $\approx 30$  % lower than  
in the case of top 100 extremes, see Supplementary Material). All of this motivates the usefulness of EGR as a predictor of  
210 extreme near surface winds and its use as a diagnostic to interpret differences between the basins in the ISCA experiments in  
Sect. 3.2.

### 3.2 ISCA experiments

First, we assess whether ISCA is a useful model to study surface wind extremes in the main storm track regions. We compute  
the winter PDFs of surface winds in the Full experiment and compare the results to ERA5. Figure 1d shows empirical PDFs  
215 of surface winds in the Full experiment. Not only is ISCA able to represent hemispheric asymmetry in extreme winds (i.e.  
stronger wind extremes in the NH, Fig. 1b), but it also correctly "ranks" the basins according to the strength of their wind  
extremes: In ISCA, the strongest wind extremes are in the NA, followed by the NP and the SO, as is consistently shown in  
reanalyses and observational products (Stanković and Caballero, 2025). Second, we analyze the annual spatial distribution of  
98th percentiles of surface winds in ISCA (Fig. 1c) and compare them to 98th percentiles in ERA5 (Fig. 1a). ISCA is able to  
220 realistically represent the spatial pattern of extreme winds. For instance, the highest values of the 98th percentiles in the NA  
are observed in the central NA region in both ERA5 and ISCA.



Having built confidence that ISCA reproduces the main characteristics of surface winds in the storm track regions across the basins, we use ISCA to further study differences between the basins. In view of the ERA5 results, the main questions we aim to answer with ISCA experiments are: why are the surface wind extremes in the storm track regions stronger in the NH than in the SH; and why are they the strongest in the NA (and not in the NP)? In particular, how do differences between the boundary conditions which characterize the storm tracks (like the presence of orography or the spatial distribution of SSTs) affect the climatological distributions of the surface wind extremes within each storm track? To address this question, we run ISCA experiments where we change the boundary conditions and test their influence on the surface wind extremes. To quantify the influence of different experiment configurations on the surface wind extremes in the storm tracks, we measure both the absolute values of the winter basin-wide 98th percentiles of near-surface winds and how much the asymmetry between the basins (difference of the basin-wide 98th percentiles of near-surface winds in the NA and SO/NP divided by SO/NP) changes percentage-wise.

Figure 5a shows the absolute values of winter basin-wide 98th percentiles of surface winds for each selected experiment and percentage-wise difference in these values between the NA and the SO (Fig. 5a, b) and the NA and the NP (Fig. 5a, c). The asymmetry between the 98th percentiles in the NA and the SO is almost completely eliminated (reduced by 83%) in the HemSymFlat experiment compared with the control experiment. The reduction in the asymmetry results from a combination of the 98th percentile decreasing in the NA and increasing in the SO. Half of the asymmetry reduction (41%) is achieved by only zonalizing SST (ZonalSST experiment) although, in this case, mainly because of a decrease in the NA. Overall, the basin-wide 98th percentile of SO surface winds gradually increases for each new experiment set-up, but the largest increase occurs with HemSymFlat experiment.

Differences in extreme winds between the two NH basins (NA and the NP) are almost completely removed (reduced by 82%) in the ZonalSST experiment. This happens because the basin-wide 98th percentile of surface winds increases in the NP, while it decreases in the NA. Flattening the orography in the HemSymFlat experiment leads to further increases in extreme winds in the NP and decreases in the NA, making the NP have stronger extreme winds than the NA.

Next, we focus on investigating the reasons behind changes in the basin-wide 98th percentiles of surface winds in different basins across the experiments. As the mid-tropospheric EGR was shown to be a good measure of the potential for cyclones to cause extreme near surface winds in ERA5, we calculate it for ISCA experiments in the same way. Figure 6 shows a scatterplot of winter basin-wide 98th percentiles of near surface winds versus winter basin-wide 98th percentiles of mid-tropospheric EGR across all the experiments in ISCA. The two quantities are tightly correlated, with a Pearson correlation coefficient of  $r = 0.97$ , significant at 1% level. This result, together with the physical arguments made in Sect. 3.1, indicates that the extreme values of EGR generally determine how extreme the near surface winds are regardless of the basin. As mentioned in Sect. 3.1, we find the same relationship in ERA5 — although absolute values of EGR and near surface winds are lower than in ISCA (see Supplementary Material).

It therefore appears that the changes in EGR between the experiments point to the characteristics of the basins which are responsible for their surface wind extremes. Furthermore, latent heat release helps to set the mean thermal structure of the troposphere, indirectly affecting EGR, meaning that EGR partly captures the role of moist processes as well. For these reasons,



we tie our analysis of basin-wide changes in extreme surface winds to changes in EGR and focus on the experiments where they differ the most from the Full experiment.

260 Zonalizing the SSTs has substantially larger influence on 98th-percentile surface winds in the NH basins than in the SH. This is not surprising, as the basins in the NH are bounded by the continents that, through warm boundary currents, influence SST distribution. However, the response of the NA differs from that of the NP. In the NA, zonalizing SSTs cools most of the NA storm tracks in a way which reduces both meridional and zonal temperature gradients. This is consistent with a weaker jet and decreased EGR in the center of the NA storm track, creating less favorable conditions for the development of extreme winds (see Fig. 7b,e,h). The basin-wide decrease of EGR in the ZonalSST simulation mainly comes from decreases in the vertical  
265 wind shear.

On the contrary, zonalization leads to increased SSTs across the NP storm track while warm regions of the tropical Pacific ocean cool (Fig. 7b). Therefore, the previously large meridional temperature gradient in the subtropical western Pacific is reduced, weakening the zonal component of the jet. As a result, the jet becomes more tilted and its orientation starts to resemble that of the NA jet (Fig. 7e). Basin-wide EGR in the NP storm track also increases—mainly as a result of an increase in the  
270 stability term, with a contribution from the shear term in some places (Fig. 7h). We conclude that the larger surface wind extremes in the NA than in the NP are mostly due to the differences in tropical and mid-latitude SST patterns between the basins.

However, zonalizing the SSTs is not enough to substantially reduce the *interhemispheric asymmetry* between extreme surface winds in the NA and the SO, which is reduced only in the HemSymFlat experiment. The rise in SO extreme winds in the  
275 HemSymFlat experiment compared with the Full experiment is consistent with an increase in EGR across the SO storm track (Fig. 7i). The increase in EGR is comprised of increases in both wind shear and stability terms, although the stability term plays a bigger role. The different SST configurations as compared to the Full experiment lead to a poleward shift of the regions with the strongest meridional temperature gradient and jet intensity (Fig. 7f). The jet also covers a broader region than in the Full and ZonalSST experiments (Fig. 7f). Following this, EGR increases across the whole SO storm track compared to both  
280 the Full and ZonalSST experiments. Basin-wide 98th percentiles of EGR and surface winds in the SO are also the largest in the HemSymFlat experiment, which subsequently reduces the interhemispheric asymmetry.

Finally, as the HemSymFlat experiment does not change SSTs in the NH relative to the ZonalSST experiment, the different response that occurs in the extreme EGR and surface winds in the NA and the NP can be primarily attributed to the orography changes. Flat orography reduces the tilt of the jet and makes it more zonally symmetric in both basins in the NH. In the NP, this  
285 is displayed as a broadening of the area with high winds present in the Full experiment. Meanwhile, the jet in the NA loses its tilt and weakens, consistent with a significant decrease of EGR extremes in the central NA.

#### 4 Summary and discussion

Our study shows that the presence of a pre-existing downstream cyclone is a distinguishing feature of cyclones associated with the top 100 extremes in surface winds in all storm track regions. Composite analysis shows that pre-existing downstream



290 cyclones are accompanied by a strong jet and upper-level PV gradients, commonly observed in cyclones associated with extreme weather (e.g., Gómara et al., 2014; Messori and Caballero, 2015). Our results indicate that there is no qualitative difference in large-scale development of top 100 extremes across the North Atlantic, North Pacific and Southern Ocean storm tracks. Thus, our study generalizes the importance of pre-existing downstream cyclones in development of cyclones associated with surface wind extremes across the hemispheres, previously documented for the North Atlantic (Stanković et al., 2024).

295 Quantitatively, however, the top 100 extremes differ across the hemispheres: specifically, in the NH they occur in the presence of stronger upper-level PV gradient, jet streak and mid-tropospheric EGR than the top 100 extremes in the SH. In addition, the percentage of top 100 extremes that develop explosively is almost two times higher in the NH. Clear differences in deepening rates helps explain why surface wind extremes are stronger in the NH than in the SH (Stanković and Caballero, 2025). Simply put, a "large-scale recipe" for generating cyclones with the largest surface wind extremes in any storm track region involves  
300 the presence of a pre-existing downstream cyclone situated poleward and eastward of an extreme-causing cyclone, whose deepening rate controls how large a surface wind extreme can be achieved. Higher rates of deepening in the NH can be linked to the higher mid-tropospheric EGR than in the SH. The EGR around top 100 extreme cyclones has its highest values around the jet streak, whose strengthening is tied to the presence of pre-existing downstream cyclones.

Simulations with ISCA further support using EGR for the purpose of analyzing surface wind extremes, as the basin-wide  
305 extreme values of EGR scale surprisingly well with the surface wind extremes across experiments. The extremes in the NA and the NP converge when extratropical and tropical SSTs are zonalized, and the interhemispheric asymmetry between the NA and the SO is reduced when extratropical and tropical SSTs are zonalized and orography is flattened. When SSTs are zonalized, the jet in the NA weakens while keeping its tilt, and extremes of surface wind and EGR weaken simultaneously. On the other hand, the jet in the NP becomes weaker, while attaining a tilt. In the NP, the new configuration of the jet happens together with  
310 the increase in the surface wind extremes, which climatologically become almost as strong as those in the NA (the NA-NP difference in extreme winds is reduced by  $\approx 82\%$ ). The jet core in the NP has climatologically higher values than the jet core in the NA in both ERA5 and ISCA, which could be an important ingredient driving NA-NP storm track differences. For example, Nakamura (1992) argued that a stronger jet core corresponds to more intense development of baroclinic wave activity up to a threshold, which the NP jet core often exceeds, after which a stronger jet core has the opposite effect. Therefore, it might not  
315 be surprising that an increase of extreme near-surface winds in the NP happens when its jet core weakens. Moreover, reduced ability of the cyclones in NP to extract potential energy has partly been tied to the characteristics of the NP jet (Schemm and Rivière, 2019).

Our results show that the reduction of interhemispheric asymmetry in extreme surface winds between the NA and SO by  $\approx 83\%$  with flat orography and zonalized, hemispherically symmetric SSTs happens through a decrease in extreme winds in  
320 the NA and an increase in the SO, consistent with an increase in EGR over the South Pacific. There are numerous studies that model the flattening of the Antarctic orography exploring a broad range of changes it causes in the SH circulation (e.g., Mechoso, 1980; Walsh et al., 2000; Singh et al., 2016; Patterson et al., 2020). Although there are differences in experiment set-ups between these studies and ours, the increase of extreme winds in the SO we observe could be tied to enhanced poleward energy and momentum transport by baroclinic eddies (Singh et al., 2016) and an increase in high-latitude eddy kinetic energy



325 when the Antarctic orography is removed (Patterson et al., 2020). On the other hand, the further decrease (increase) in the  
zonalized SST experiment of the extreme winds over the NA (the NP) when the orography is flat shows that the orography also  
plays a role in shaping the extremes of the NH. The experiment with flat orography, however, exhibits non-linear effects on the  
NH storm track, as a decrease of extreme winds in the NA, for example, happens only with zonalized SSTs (flat orography and  
non-zonalized SSTs cause a slight increase in extreme winds over the NA). These results provide insight into how orography  
330 might influence NH near-surface wind extremes, thus complementing a vast body of previous work on disentangling the  
influence of orography on mean characteristics of large-scale circulation in the NH (e.g., Brayshaw et al., 2009; White et al.,  
2021; Shaw et al., 2022).

It is worth noting some of the limitations of our results. Our focus on the large scales means we do not consider mesoscale  
or boundary-layer processes which can play an important complementary role in generating surface wind extremes (Hewson  
and Neu, 2015). In addition, the most prominent feature for the top 100 extremes is the presence of a pre-existing downstream  
cyclone. Our results mainly focused on the role of this pre-existing cyclone in generating a large-scale environment suitable  
for development of top 100 extremes, without considering the merging and cyclone-cyclone interaction between extreme  
and pre-existing cyclones. Further, although the ISCA model is able to represent the main features of the Earth's climate  
relevant for our study (like PDFs of surface winds in the storm track regions), it is not clear how reliable it is in realistically  
340 representing individual cyclones. ISCA also has some known biases relevant to storm track behavior. For example, like many  
other climate models (Shaw et al., 2016; Patterson et al., 2020), it has a jet that is too zonal and located more equatorward than  
in the observations. Finally, ISCA does not have a realistic representation of clouds, which possibly limits an extension of our  
analysis to project the changes in the storm track with anthropogenic warming, as biases in cloud representation are one of the  
main uncertainty sources relevant for storm tracks (Shaw et al., 2016).

345 Finally, there are approaches that can be applied to extend the results from our study. The study could be complemented by  
the inclusion of other extremes, like precipitation extremes, that often accompany cyclones that cause extreme winds (Pfahl and  
Sprenger, 2016; Cornér et al., 2025). Although less frequently, some extreme surface winds associated with cyclones happen  
outside winter seasons (especially in the SH, e.g., Stanković and Caballero (2025)) and an analysis of large-scale characteristics  
of cyclones in seasons other than winter could generalize the understanding of cyclones that cause extreme surface winds.  
350 When it comes to modeling, a next step could be to test whether one of our main results that extreme basin-wide EGR scales  
with the extreme surface winds holds in more complex, coupled climate models or in climates that greatly differ from the  
present one. Other approaches, like those applying energetic frameworks, are better suited than EGR-like metrics to represent  
mean storm track activity in climates of snowball Earth (Shaw and Graham, 2020) or with an intense warming (Shaw et al.,  
2018). It could be beneficial to contrast usefulness of these zonal-mean metrics in representing surface wind extremes with  
355 our analysis focused on basin-wide metrics. Examining how the cyclones that cause surface wind extremes would change with  
projected future climates could employ the use of models with high resolution (like for e.g., Gentile et al., 2023, 2025), focus  
on compound extremes related to explosively deepening cyclones (e.g., Lopez-Marti et al., 2025) or leverage understanding  
that comes from idealized climate simulations (e.g., Sinclair and Catto, 2023; Bouvier et al., 2025).



## 5 Conclusions

360 In this study, we analyze historical extratropical cyclones associated with the 100 most extreme surface winds over the North Atlantic, North Pacific and Southern Ocean storm tracks. Our study is motivated by the observation that such surface wind extremes are more intense in the NH, and in particular in the North Atlantic, than in the SH. We employ composite analysis to study the large-scale features of the flow around these cyclones and we perform modeling experiments to examine differences in characteristics of the storm track basins relevant for surface wind extremes. Finally, we answer the questions posed in the Introduction as follows:

- 370 1. The presence of a pre-existing downstream cyclone is a key large-scale feature of the development of cyclones associated with the top 100 most extreme surface winds in all storm track basins. Pre-existing cyclones are situated poleward and eastward of developing top 100 extremes and they intensify strong jet streaks and upper-level potential vorticity gradients within which the top 100 extremes develop. After crossing the jet streak, at the time of the maximum surface wind severity, the top 100 extremes merge with pre-existing downstream cyclones to form a large area of negative mean sea-level pressure anomalies.
- 375 2. Large-scale differences between the basins are quantitative. Though composite analysis shows qualitatively similar development of the top 100 extremes in different basins, those in the northern hemisphere deepen more explosively and are surrounded by higher values of mid-tropospheric Eady growth rates. The highest values of Eady growth rates are primarily found around the jet streaks, which are stronger in the northern hemisphere where surface wind extremes are higher.
- 380 3. Idealized modeling experiments with different boundary conditions show a strong positive correlation between basin-wide extreme surface winds and basin-wide extreme Eady growth rates. The North Atlantic has highest extreme winds and Eady growth rates, but they become almost equal to those in the North Pacific when inter-basing sea-surface temperature differences are removed by zonalizing them across the tropics and extratropics. On the other hand, the interhemispheric asymmetry in extreme surface winds between the North Atlantic and the Southern Ocean is greatly reduced once sea-surface temperatures are zonalized, made hemispherically symmetric and the orography is flattened.

*Data availability.* Data from ERA5 reanalysis used in the study was downloaded from <https://doi.org/10.24381/cds.bd0915c6> (Accessed on 23-03-2026) (Hersbach et al., 2023a) for pressure levels and <https://doi.org/10.24381/cds.adbb2d47> (Accessed on 23-03-2026) (Hersbach et al., 2023b) for single levels. The cyclone tracking data was downloaded from <https://doi.org/10.17043/beran-2024-era5-cyclone-tracking-1> (Accessed on 23-03-2026) (Beran et al., 2024). The code for the ISCA model (Vallis et al., 2018) is publicly available at <https://execlim.github.io/IscaWebsite/index.html>. The model was run in the standard realistic continents configuration and the input files with the prescribed sea-surface temperatures used to run ISCA experiments are made available in a Zenodo repository available at <https://doi.org/10.5281/zenodo.19184262> (Accessed on 23-03-2026).



*Author contributions.* AS, RC, and GM designed the study. AS carried out the analysis and drafted the first version of the manuscript. All authors contributed to discussions, structuring the analysis, and reviewing the paper.

*Competing interests.* No competing interests are present.

395 *Acknowledgements.* AS wants to thank Ryan Boukrouche and Neil Lewis for discussions around the ISCA model. This research has been supported by the Horizon 2020 framework programme H2020 Excellent Science (Marie Skłodowska-Curie grant agreement no. 956396, EDIPI project). GM acknowledges the support of the Swedish Research Council Vetenskapsrådet (grant no. 2022-06599). Part of the data handling was enabled by resources provided by the National Academic Infrastructure for Supercomputing in Sweden (NAISS), partially funded by the Swedish Research Council through grant agreement no. 2022-06725.



## References

- 400 Bengtsson, L., Hodges, K. I., Esch, M., Keenlyside, N., Kornbluh, L., LUO, J.-J., and Yamagata, T.: How may tropical cyclones change in a warmer climate?, *Tellus a*, 59, 539–561, 2007.
- Beran, J., Bin Masood, T., Engelke, W., Svensson, G., Caballero, R., and Hotz, I.: Hourly ERA5 cyclone tracking data from 1979–2020 using topological methods. Dataset version 1 [Dataset], <https://doi.org/https://doi.org/10.17043/beran-2024-era5-cyclone-tracking-1>, 2024.
- Besson, P., Fischer, L. J., Schemm, S., and Sprenger, M.: A global analysis of the dry-dynamic forcing during cyclone growth and propagation, *Weather and Climate Dynamics Discussions*, 2021, 1–25, 2021.
- 405 Bouvier, C., Cornér, J., Toropainen, A., Bowery, A., Carver, G., Sparrow, S., Wallom, D., and Sinclair, V. A.: Baroclinic wave simulation ensemble: a machine learning ready dataset, *Scientific data*, 12, 1811, 2025.
- Brayshaw, D. J., Hoskins, B., and Blackburn, M.: The basic ingredients of the North Atlantic storm track. Part I: Land–sea contrast and orography, *Journal of the Atmospheric Sciences*, 66, 2539–2558, 2009.
- 410 Brayshaw, D. J., Hoskins, B., and Blackburn, M.: The basic ingredients of the North Atlantic storm track. Part II: Sea surface temperatures, *Journal of the Atmospheric Sciences*, 68, 1784–1805, 2011.
- Cardone, V., Callahan, B., Chen, H., Cox, A., Morrone, M., and Swail, V.: Global distribution and risk to shipping of very extreme sea states (VESS), *International Journal of Climatology*, 35, 2015.
- Catto, J., Jakob, C., Berry, G., and Nicholls, N.: Relating global precipitation to atmospheric fronts, *Geophysical Research Letters*, 39, 2012.
- 415 Catto, J. L., Shaffrey, L. C., and Hodges, K. I.: Can climate models capture the structure of extratropical cyclones?, *Journal of Climate*, 23, 1621–1635, 2010.
- Catto, J. L., Ackerley, D., Booth, J. F., Champion, A. J., Colle, B. A., Pfahl, S., Pinto, J. G., Quinting, J. F., and Seiler, C.: The future of midlatitude cyclones, *Current Climate Change Reports*, 5, 407–420, 2019.
- Chemke, R., Ming, Y., and Yuval, J.: The intensification of winter mid-latitude storm tracks in the Southern Hemisphere, *Nat. Clim. Change*, 12, 553–557, 2022.
- 420 Clough, S. A., Shephard, M. W., Mlawer, E. J., Delamere, J., Iacono, M. J., Cady-Pereira, K., Boukabara, S., and Brown, P. D.: Atmospheric radiative transfer modeling: A summary of the AER codes, *Journal of Quantitative Spectroscopy and Radiative Transfer*, 91, 233–244, 2005.
- Cornér, J., Bouvier, C., Doiteau, B., Pantillon, F., and Sinclair, V. A.: Classification of North Atlantic and European extratropical cyclones using multiple measures of intensity, *Natural Hazards and Earth System Sciences*, 25, 207–229, 2025.
- 425 Dacre, H., Hawcroft, M., Stringer, M., and Hodges, K.: An extratropical cyclone atlas: A tool for illustrating cyclone structure and evolution characteristics, *Bulletin of the American Meteorological Society*, 93, 1497–1502, 2012.
- Donelan, M. A., Dobson, F. W., Smith, S. D., and Anderson, R. J.: On the dependence of sea surface roughness on wave development, *Journal of physical Oceanography*, 23, 2143–2149, 1993.
- 430 Dowdy, A. J. and Catto, J. L.: Extreme weather caused by concurrent cyclone, front and thunderstorm occurrences, *Scientific Reports*, 7, 40359, 2017.
- Engelke, W., Masood, T. B., Beran, J., Caballero, R., and Hotz, I.: Topology-based feature design and tracking for multi-center cyclones, in: *Topological Methods in Data Analysis and Visualization VI: Theory, Applications, and Software*, pp. 71–85, Springer, 2021.
- Frierson, D. M., Held, I. M., and Zurita-Gotor, P.: A gray-radiation aquaplanet moist GCM. Part I: Static stability and eddy scale, *Journal of the atmospheric sciences*, 63, 2548–2566, 2006.
- 435

Gentile, E. S., Zhao, M., and Hodges, K.: Poleward intensification of midlatitude extreme winds under warmer climate, *npj Climate and Atmospheric Science*, 6, 219, 2023.

440 Gentile, E. S., Harris, L., Zhao, M., Hodges, K., Tan, Z., Cheng, K.-Y., and Zhou, L.: Response of extreme north Atlantic midlatitude cyclones to a warmer climate in the GFDL X-SHIELD kilometer-scale global storm-resolving model, *Geophys. Res. Lett.*, 52, e2024GL112570, 2025.

Gómara, I., Pinto, J. G., Woollings, T., Masato, G., Zurita-Gotor, P., and Rodríguez-Fonseca, B.: Rossby wave-breaking analysis of explosive cyclones in the Euro-Atlantic sector, *Quarterly Journal of the Royal Meteorological Society*, 140, 738–753, 2014.

Hanley, J. and Caballero, R.: Objective identification and tracking of multicentre cyclones in the ERA-Interim reanalysis dataset, *Quarterly Journal of the Royal Meteorological Society*, 138, 612–625, 2012a.

445 Hanley, J. and Caballero, R.: The role of large-scale atmospheric flow and Rossby wave breaking in the evolution of extreme windstorms over Europe, *Geophysical Research Letters*, 39, <https://doi.org/10.1029/2012GL053408>, 2012b.

Hersbach, H., Bell, B., Berrisford, P., Hirahara, S., Horányi, A., Muñoz-Sabater, J., Nicolas, J., Peubey, C., Radu, R., Schepers, D., Simmons, A., Soci, C., Abdalla, S., Abellan, X., Balsamo, G., Bechtold, P., Biavati, G., Bidlot, J., Bonavita, M., Chiara, G. D., Dahlgren, P., Dee, D., Diamantakis, M., Dragani, R., Flemming, J., Forbes, R., Fuentes, M., Geer, A., Haimberger, L., Healy, S., Hogan, R. J., Hólm, E.,  
450 Janisková, M., Keeley, S., Laloyaux, P., Lopez, P., Lupu, C., Radnoti, G., de Rosnay, P., Rozum, I., Vamborg, F., Villaume, S., and Thépaut, J.-N.: The ERA5 global reanalysis [Dataset], *Quart. J. Roy. Meteor. Soc.*, 146, 1999–2049, <https://doi.org/10.24381/cds.adbb2d47>, 2020.

Hersbach, H., Bell, B., Berrisford, P., Biavati, G., Horányi, A., Muñoz Sabater, J., Nicolas, J., Peubey, C., Radu, R., Rozum, I., Schepers, D., Simmons, A., Soci, C., Dee, D., and Thépaut, J.-N.: ERA5 hourly data on pressure levels from 1940 to present, Copernicus Climate Change Service (C3S) Climate Data Store (CDS) [Dataset], <https://doi.org/10.24381/cds.bd0915c6>, 2023a.

455 Hersbach, H., Bell, B., Berrisford, P., Biavati, G., Horányi, A., Muñoz Sabater, J., Nicolas, J., Peubey, C., Radu, R., Rozum, I., Schepers, D., Simmons, A., Soci, C., Dee, D., and Thépaut, J.-N.: ERA5 hourly data on single levels from 1940 to present, Copernicus Climate Change Service (C3S) Climate Data Store (CDS) [Dataset], <https://doi.org/10.24381/cds.adbb2d47>, 2023b.

Hewson, T. D. and Neu, U.: Cyclones, windstorms and the IMILAST project, *Tellus A: Dyn. Meteorol. Oceanogr.*, 67, 27–128, 2015.

Hoskins, B. J. and Hodges, K. I.: New perspectives on the Northern Hemisphere winter storm tracks, *J. Atmos. Sci.*, 59, 1041–1061, 2002.

460 Hoskins, B. J. and Hodges, K. I.: A new perspective on Southern Hemisphere storm tracks, *J. Clim.*, 18, 4108–4129, 2005.

Hsiung, J.: Mean surface energy fluxes over the global ocean, *Journal of Geophysical Research: Oceans*, 91, 10585–10606, 1986.

Klawa, M. and Ulbrich, U.: A model for the estimation of storm losses and the identification of severe winter storms in Germany, *Natural Hazards and Earth System Sciences*, 3, 725–732, 2003.

465 Lacour, L., Ardyna, M., Stec, K., Claustre, H., Prieur, L., Poteau, A., D’Alcala, M. R., and Iudicone, D.: Unexpected winter phytoplankton blooms in the North Atlantic subpolar gyre, *Nature Geoscience*, 10, 836–839, 2017.

Laurila, T. K., Gregow, H., Cornér, J., and Sinclair, V. A.: Characteristics of extratropical cyclones and precursors to windstorms in northern Europe, *Weather and Climate Dynamics*, 2, 1111–1130, 2021.

Leckebusch, G., Renggli, D., and Ulbrich, U.: Development and application of an objective storm severity measure for the Northeast Atlantic region, *Meteorologische Zeitschrift*, 17, 575–587, 2008.

470 Liu, W. T., Tang, W., and Xie, X.: Wind power distribution over the ocean, *Geophysical research letters*, 35, 2008.

Lopez-Marti, F., Ginesta, M., Faranda, D., Rutgersson, A., Yiou, P., Wu, L., and Messori, G.: Future changes in compound explosive cyclones and atmospheric rivers in the North Atlantic, *Earth System Dynamics*, 16, 169–187, 2025.



- Mechoso, C. R.: The atmospheric circulation around Antarctica: Linear stability and finite-amplitude interactions with migrating cyclones, *Journal of Atmospheric Sciences*, 37, 2209–2233, 1980.
- 475 Messmer, M. and Simmonds, I.: Global analysis of cyclone-induced compound precipitation and wind extreme events, *Weather and Climate Extremes*, 32, 100324, 2021.
- Messori, G. and Caballero, R.: On double Rossby wave breaking in the North Atlantic, *Journal of Geophysical Research: Atmospheres*, 120, 11–129, 2015.
- Moemken, J., Alifdini, I., Ramos, A. M., Georgiadis, A., Brocklehurst, A., Braun, L., and Pinto, J. G.: Insurance loss model vs meteorological  
480 loss index—How comparable are their loss estimates for European windstorms?, *Natural Hazards and Earth System Sciences Discussions*, 2024, 1–19, 2024.
- Nakamura, H.: Midwinter suppression of baroclinic wave activity in the Pacific, *Journal of Atmospheric Sciences*, 49, 1629–1642, 1992.
- Neu, U., Akperov, M. G., Bellenbaum, N., Benestad, R., Blender, R., Caballero, R., Coccozza, A., Dacre, H. F., Feng, Y., Fraedrich, K.,  
485 Grieger, J., Gulev, S., Hanley, J., Hewson, T., Inatsu, M., Keay, K., Kew, S. F., Kindem, I., Leckebusch, G. C., Liberato, M. L. R., Lionell,  
P., Mokhov, I. I., Pinto, J. G., Raible, C. C., Real, M., Rudeva, I., Schuster, M., Simmonds, I., Sinclai, M., Sprenger, M., Tilinina, N. D.,  
Trigo, I. F., Ulbrich, S., Ulbrich, U., Wang, X. L., and Wernli, H.: IMILAST: A community effort to intercompare extratropical cyclone  
detection and tracking algorithms, *BAMS*, 94, 529–547, 2013.
- Nilsson, E., Lukaszczuk, J., Engelke, W., Masood, T. B., Svensson, G., Caballero, R., Garth, C., and Hotz, I.: Exploring cyclone evolution  
with hierarchical features, in: *2022 Topological Data Analysis and Visualization (TopoInVis)*, pp. 92–102, IEEE, 2022.
- 490 Patterson, M., Woollings, T., Bracegirdle, T. J., and Lewis, N. T.: Wintertime Southern Hemisphere jet streams shaped by interaction of  
transient eddies with Antarctic orography, *Journal of Climate*, 33, 10505–10522, 2020.
- Pfahl, S. and Sprenger, M.: On the relationship between extratropical cyclone precipitation and intensity, *Geophysical Research Letters*, 43,  
1752–1758, 2016.
- Pfahl, S. and Wernli, H.: Quantifying the relevance of cyclones for precipitation extremes, *Journal of Climate*, 25, 6770–6780, 2012.
- 495 Sanders, F. and Gyakum, J. R.: Synoptic-dynamic climatology of the “bomb”, *Monthly Weather Review*, 108, 1589–1606, 1980.
- Schemm, S. and Rivière, G.: On the efficiency of baroclinic eddy growth and how it reduces the North Pacific storm-track intensity in  
midwinter, *Journal of Climate*, 32, 8373–8398, 2019.
- Seneviratne, S. I., Zhang, X., Adnan, M., Badi, W., Dereczynski, C., Luca, A. D., Ghosh, S., Iskandar, I., Kossin, J., Lewis, S., et al.: Weather  
and climate extreme events in a changing climate, 2021.
- 500 Shaw, T., Baldwin, M., Barnes, E. A., Caballero, R., Garfinkel, C., Hwang, Y.-T., Li, C., O’gorman, P., Rivière, G., Simpson, I., , and Voigt,  
A.: Storm track processes and the opposing influences of climate change, *Nature Geosci.*, 9, 656–664, 2016.
- Shaw, T. A. and Graham, R. J.: Hydrological cycle changes explain weak Snowball Earth storm track despite increased surface baroclinicity,  
*Geophysical Research Letters*, 47, e2020GL089866, 2020.
- Shaw, T. A., Barpanda, P., and Donohoe, A.: A moist static energy framework for zonal-mean storm-track intensity, *Journal of the Atmo-  
505 spheric Sciences*, 75, 1979–1994, 2018.
- Shaw, T. A., Miyawaki, O., and Donohoe, A.: Stormier Southern Hemisphere induced by topography and ocean circulation, *Proc. Natl. Acad.  
Sci.*, 119, e2123512119, 2022.
- Shimkus, C. E., Ting, M., Booth, J. F., Adamo, S. B., Madajewicz, M., Kushnir, Y., and Rieder, H. E.: Winter storm intensity, hazards, and  
property losses in the New York tristate area, *Annals of the New York Academy of Sciences*, 1400, 65–80, 2017.



- 510 Simmonds, I. and Lim, E.-P.: Biases in the calculation of Southern Hemisphere mean baroclinic eddy growth rate, *Geophysical Research Letters*, 36, 2009.
- Sinclair, V. A. and Catto, J. L.: The relationship between extra-tropical cyclone intensity and precipitation in idealised current and future climates, *Weather and Climate Dynamics*, 4, 567–589, 2023.
- Singh, H. K., Bitz, C. M., and Frierson, D. M.: The global climate response to lowering surface orography of Antarctica and the importance  
515 of atmosphere–ocean coupling, *Journal of Climate*, 29, 4137–4153, 2016.
- Stanković, A. and Caballero, R.: Surface wind extremes are stronger in the Northern Hemisphere Oceans than in the Southern Ocean, *Geophysical Research Letters*, 52, e2025GL118 024, 2025.
- Stanković, A., Messori, G., Pinto, J. G., and Caballero, R.: Large-scale perspective on extreme near-surface winds in the central North Atlantic, *WCD*, 5, 821–837, 2024.
- 520 Taylor, K. E.: The sea surface temperature and sea-ice concentration boundary conditions for AMIP II simulations, Program for Climate Model Diagnosis and Intercomparison, Lawrence River, 2000.
- Thomson, S. I. and Vallis, G. K.: Atmospheric response to SST anomalies. Part I: Background-state dependence, teleconnections, and local effects in winter, *Journal of the Atmospheric Sciences*, 75, 4107–4124, 2018a.
- Thomson, S. I. and Vallis, G. K.: Atmospheric response to SST anomalies. Part II: Background-state dependence, teleconnections, and local  
525 effects in summer, *Journal of the Atmospheric Sciences*, 75, 4125–4138, 2018b.
- Ulbrich, U., Leckebusch, G. C., and Donat, M. G.: Windstorms, the most costly natural hazard in Europe, *Natural disasters and adaptation to climate change*. Cambridge University Press, Cambridge, pp. 109–120, 2013a.
- Ulbrich, U., Leckebusch, G. C., Grieger, J., Schuster, M., Akperov, M., Bardin, M. Y., Feng, Y., Gulev, S., Inatsu, M., Keay, K., Kew, S. F., Liberato, M. L. R., Lionello, P., Mokhov, I. I., Neu, U., Pinto, J. G., Raible, C. C., Reale, M., Rudeva, I., Simmonds, I., Tilinina, N. D.,  
530 Trigo, I. F., Ulbrich, S., Wang, X. L., and Wernli, H.: Are greenhouse gas signals of Northern Hemisphere winter extra-tropical cyclone activity dependent on the identification and tracking algorithm?, *Meteorologische Zeitschrift*, 22, 61–68, 2013b.
- Vallis, G. K., Colyer, G., Geen, R., Gerber, E., Jucker, M., Maher, P., Paterson, A., Pietschnig, M., Penn, J., and Thomson, S. I.: Isca, v1. 0: A framework for the global modelling of the atmospheres of Earth and other planets at varying levels of complexity, *Geoscientific Model Development*, 11, 843–859, 2018.
- 535 Walsh, K. J., Simmonds, I., and Collier, M.: Sigma-coordinate calculation of topographically forced baroclinicity around Antarctica, *Dynamics of atmospheres and oceans*, 33, 1–29, 2000.
- Wanninkhof, R. and McGillis, W. R.: A cubic relationship between air-sea CO<sub>2</sub> exchange and wind speed, *Geophysical Research Letters*, 26, 1889–1892, 1999.
- White, I. P., Lachmy, O., and Harnik, N.: Influence of a local diabatic heating source on the midlatitude circulation, *Quarterly Journal of the Royal Meteorological Society*, 150, 5167–5187, 2024.
- 540 White, R. H., Wallace, J. M., and Battisti, D.: Revisiting the role of mountains in the Northern Hemisphere winter atmospheric circulation, *Journal of the Atmospheric Sciences*, 78, 2221–2235, 2021.
- Wilks, D.: “The stippling shows statistically significant grid points”: How research results are routinely overstated and overinterpreted, and what to do about it, *Bulletin of the American Meteorological Society*, 97, 2263–2273, 2016.

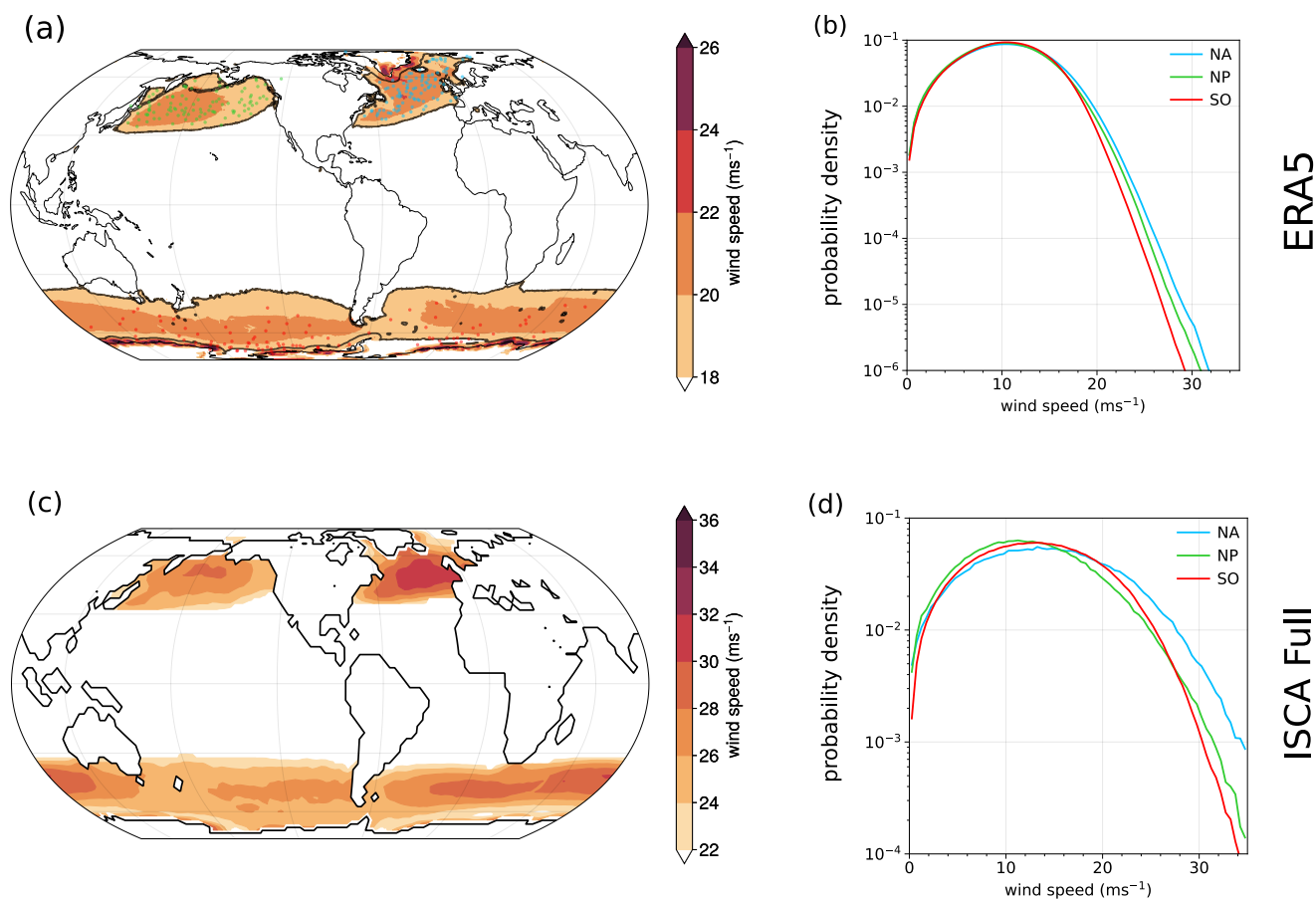


**Figure 1.** Maps of annual 98th percentile (a,c) and probability density functions (b,d) of daily-maximum and 6-hourly (a,b) 10-m windspeed in ERA5 and (c,d) windspeed at the level closest to the surface in ISCA Full experiment, respectively. Probability density functions are made from windspeed sampled in the regions marked in (a) and (c) in the North Atlantic (NA, blue), North Pacific (NP, green) and Southern Ocean (SO, red). Black contours in (a) show the selected storm track regions used for calculating severity in ERA5, while the selected storm track regions in ISCA correspond to the colored areas in (a). Green, blue and red dots over the storm track regions in (a) show the locations of cyclone centers of the top 100 extremes at the time of maximum severity.

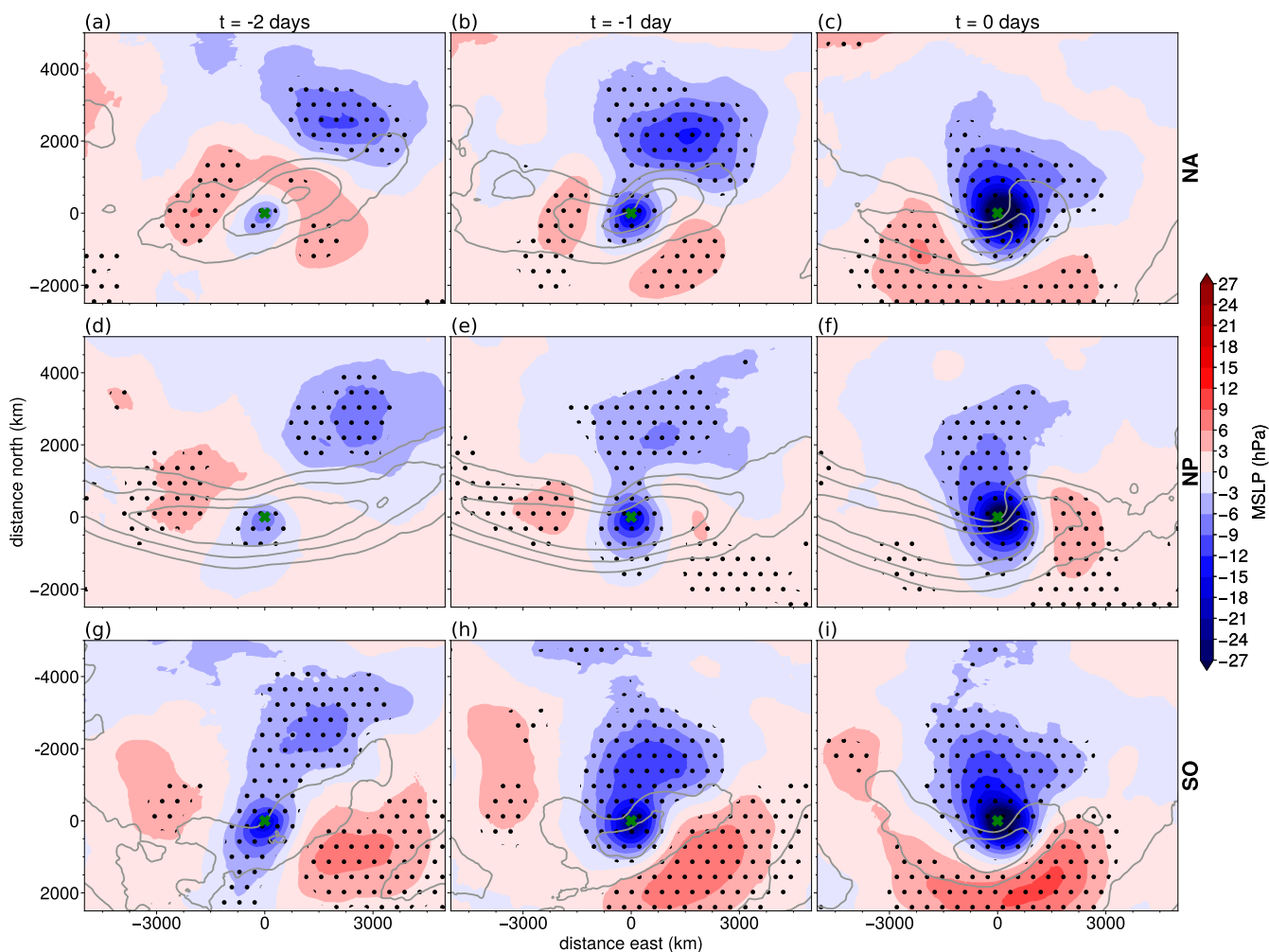


**Figure 2.** Composite MSLP anomalies in ERA5 relative to the 1979-2020 climatology for top 100 extremes in the NA (a-c), NP (d-f) and SO (g-i) centered on the cyclone locations from  $t = -2$  days to  $t = 0$  days. Lags are relative to the time of maximum 10-m wind speeds on the day with maximum severity. Green crosses denote locations of cyclone centers of top 100 extremes. Grey contours show the values of 250 hPa wind speeds, starting from  $35 \text{ ms}^{-1}$  and increasing in steps of  $10 \text{ ms}^{-1}$ . Black dots show areas where MSLP anomalies are statistically significant at the 1 % level and corrected for false discovery (Wilks, 2016).

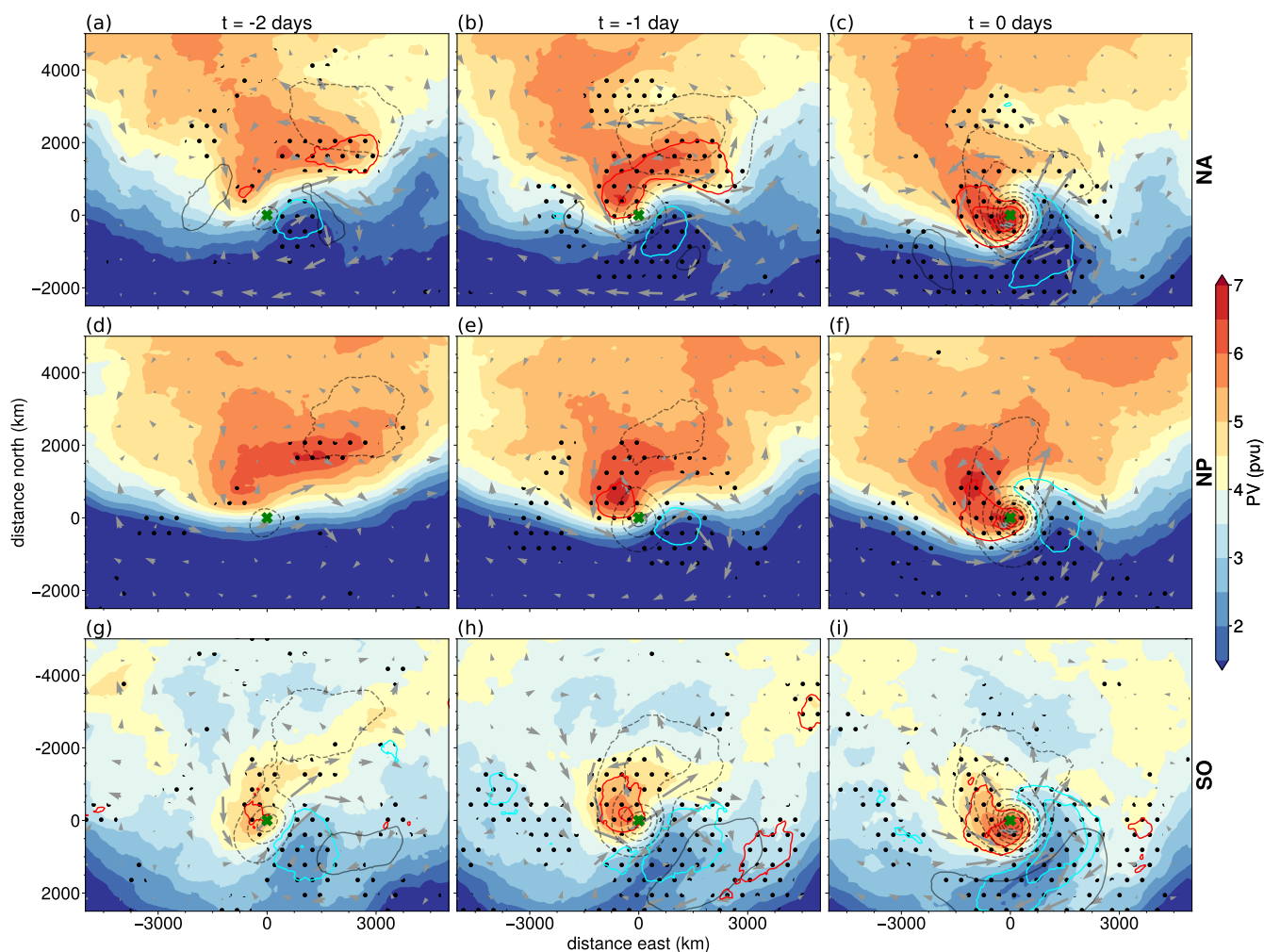


**Figure 3.** Upper-level composites for top 100 extremes in the NA (a-c), NP (d-f) and SO (g-i) centered on the cyclone locations from  $t = -2$  days to  $t = 0$  days. Colors show upper level PV (200-300 hPa mean) values, while red and blue contours show positive and negative upper level PV anomalies relative to the 1979-2020 climatology, respectively, every  $\pm 1$  pvu and starting from  $\pm 1$  pvu. Grey arrows show 250 hPa horizontal wind speed anomalies from climatology. Black contours show MSLP anomalies relative to the 1979-2020 climatology, every  $\pm 5$  hPa and starting from  $\pm 5$  hPa (dashed for negative anomalies). Green crosses have the same meaning as in Figure 2. Black dots show areas where upper level PV anomalies are statistically significant at the 1 % level and corrected for false discovery (Wilks, 2016).

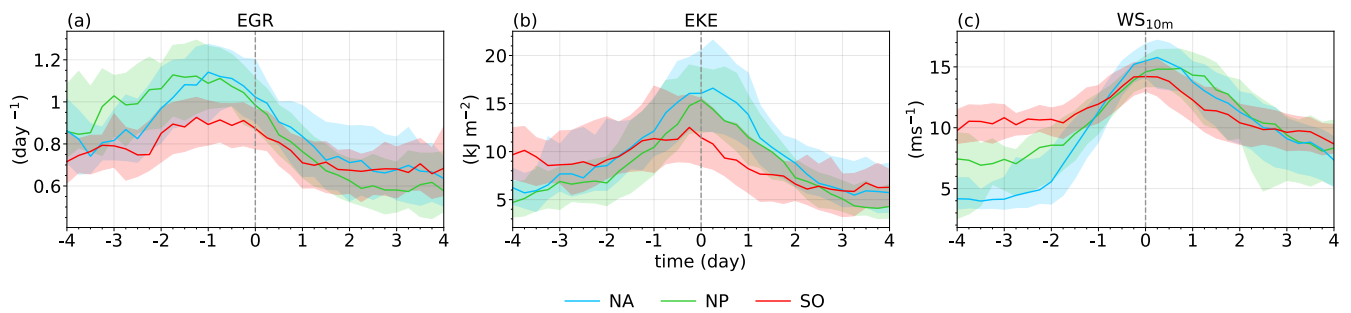


**Figure 4.** Time-evolution of median values in the 1000-km footprint around top 100 extremes of mid-tropospheric Eady growth rate (a), vertically integrated eddy kinetic energy (b) and 10-m wind speed (c). Colors signify the same basins as in Fig. 1a, while shading in (a-c) shows the area between 25th and 75th percentiles.

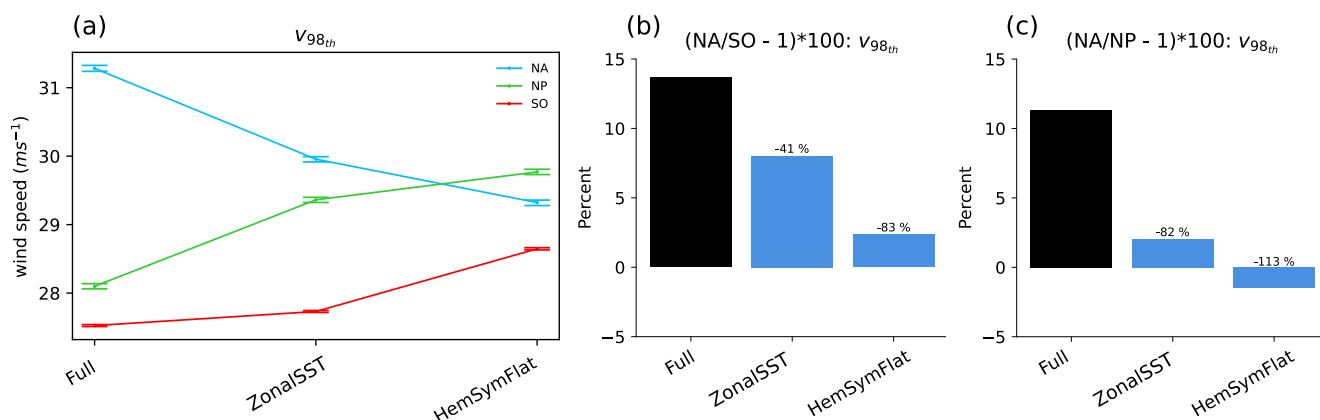


**Figure 5.** Absolute values of basin-wide 98th percentiles of surface wind speeds (a) and the relative difference in the percentile values between the North Atlantic and the Southern Ocean (b) and the North Atlantic and the North Pacific (c) with the selected ISCA experiments. Colors in (a) signify the same basins as in Fig. 1c and 4, while the horizontal lines above each value show the confidence interval at 1 % significance level computed with resampling 10000 times. Percentage values above certain bars in (b) and (c) show a percentage difference in asymmetries compared to the Full ISCA experiment.

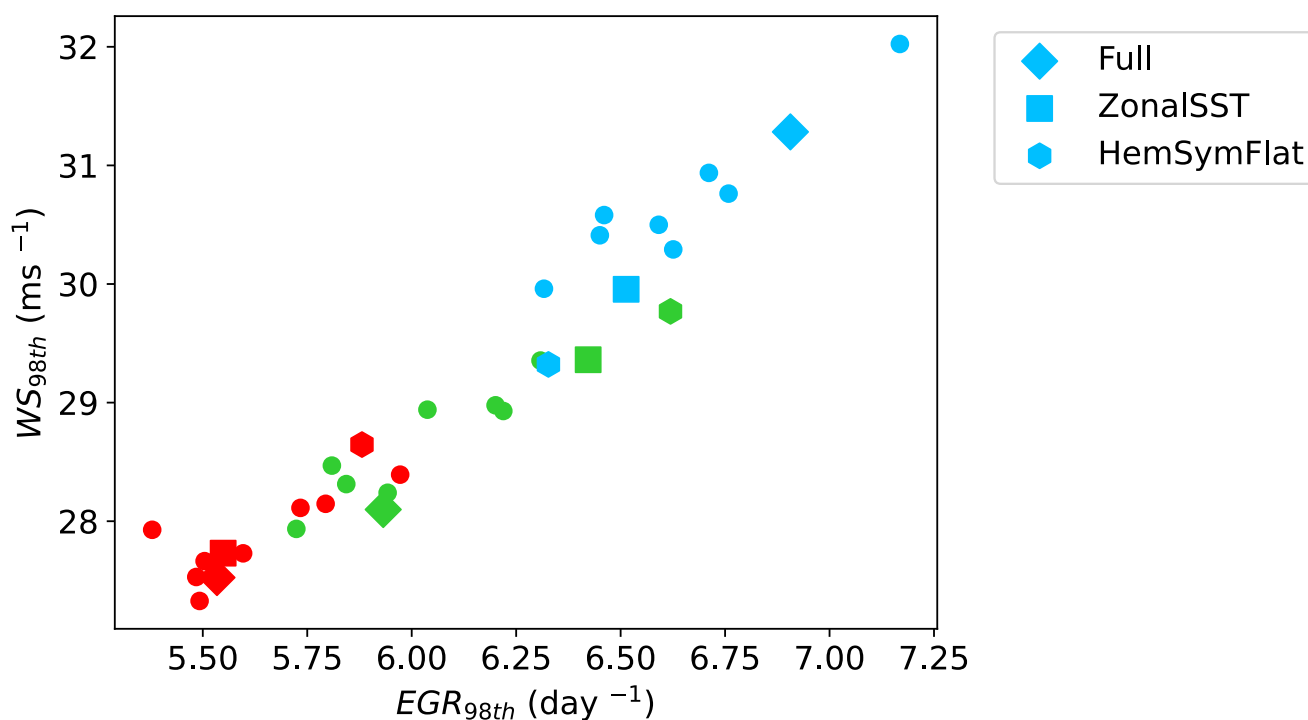


**Figure 6.** Scatterplot of winter basin-wide 98th percentiles of near-surface wind speed (y-axis) versus winter basin-wide 98th percentiles of mid-tropospheric Eady growth rates (x-axis) across 11 different ISCA experiments with varying boundary conditions. Different colors represent different basins (same colors as in Fig. 1c, 4, 5a), while shapes different than simple dots represent experiments chosen for the analysis.

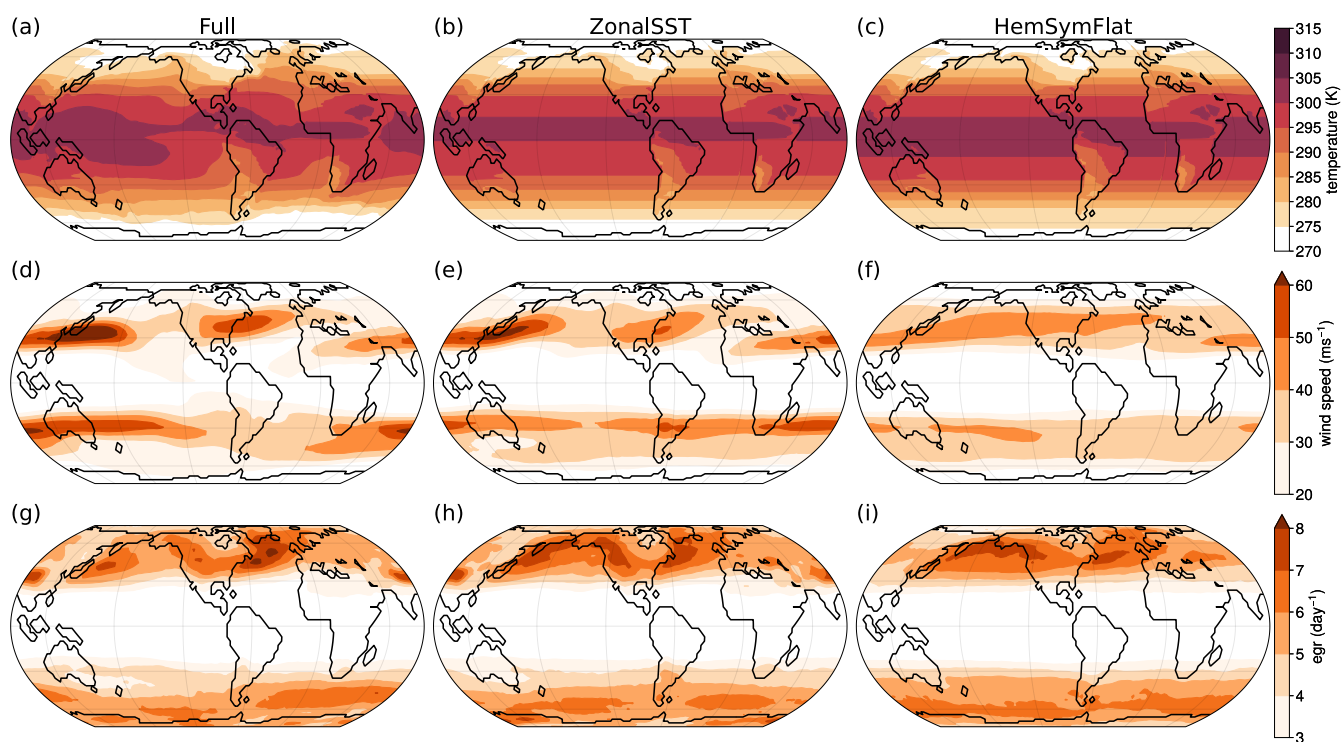


**Figure 7.** Climatologies of SSTs (a-c), medians of wind speed between 200 and 300 hPa (d-f) and EGR (g-i) during respective winter seasons across ISCA experiments. (a), (d), (g) show the results from Full, (b), (e), (h) ZonalSST and (c), (f), (i) HemSymFlat experiments.